Tilted Wheel Satellite Attitude Control with Air-Bearing Table Experimental Results

Inumoh, LO, Forshaw, JL & Horri, NM

Original citation & hyperlink:
Inumoh, LO, Forshaw, JL & Horri, NM 2015, 'Tilted Wheel Satellite Attitude Control with Air-Bearing Table Experimental Results' Acta Astronautica, vol 117, no. Article 5550, pp. 414-429. DOI: 10.1016/j.actaastro.2015.09.007
https://dx.doi.org/10.1016/j.actaastro.2015.09.007

DOI 10.1016/j.actaastro.2015.09.007
ISSN 0094-5765)

Publisher: Elsevier

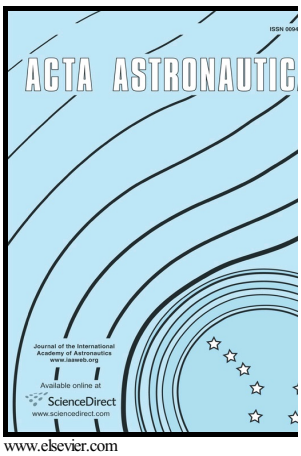

Tilted Wheel Satellite Attitude Control with Air-Bearing Table Experimental Results

Lawrence O. Inumoh, Jason L. Forshaw, Nadjim M. Horri

PII: S0094-5765(15)00349-5
DOI: http://dx.doi.org/10.1016/j.actaastro.2015.09.007
Reference: AA5550

To appear in: *Acta Astronautica*

Received date: 23 February 2015
Revised date: 9 May 2015
Accepted date: 14 September 2015

Cite this article as: Lawrence O. Inumoh, Jason L. Forshaw and Nadjim M Horri, Tilted Wheel Satellite Attitude Control with Air-Bearing Table Experimental Results, *Acta Astronautica* http://dx.doi.org/10.1016/j.actaastro.2015.09.007

Acta Astronautica

Tilted Wheel Satellite Attitude Control with Air-Bearing Table Experimental Results

Lawrence O. Inumoh[1], Jason L. Forshaw[2,*]

Surrey Space Centre, Department of Electronic Engineering, University of Surrey, Guildford, GU2 7XH, UK

Nadjim M. Horri[3,*]

Aeronautical, Aviation, Electronic & Electrical (AAEE), Coventry University, Coventry, CV1 5FB, UK

Abstract

Gyroscopic actuators for satellite control have attracted significant research interest over the years, but their viability for the control of small satellites has only recently started to become clear. Research on variable speed gyroscopic actuators has long been focused on single gimbal actuators; double gimbal actuators typically operate at constant wheel spin rate and allow tilt angle ranges far larger than the ranges needed to operate most satellite missions. This research examines a Tilted Wheel, a newly proposed type of inertial actuator that can generate torques in all three principal axes of a rigid satellite using a spinning wheel and a double tilt mechanism. The tilt mechanism tilts the angular momentum vector about two axes providing two degree of freedom control, while variation of the wheel speed provides the third. The equations of motion of the system lead to a singularity-free system during nominal operation avoiding the need for complex steering logic. This paper describes the hardware design of the Tilted Wheel and the experimental setup behind both standalone and spherical air-bearing tables used to test it. Experimental results from the air bearing table are provided with the results depicting the high performance capabilities of the proposed actuator in torque generation.

Keywords: attitude control, CMG, actuator design, testbed design, air bearing table

Nomenclature

δ	= Control signal (generic)
α, β	= Tilted wheel attitude (in W)
$\dot{\alpha}$, $\dot{\beta}$	= Tilted wheel attitude rates (in W)
B	= Satellite body frame
$\dot{\boldsymbol{H}} = [\dot{H}_1, \dot{H}_2, \dot{H}_3]$	= Overall torque (in B)
$\boldsymbol{H} = [H_1, H_2, H_3]$	= Angular momentum (in B)
$\dot{\boldsymbol{h}} = [\dot{h}_1, \dot{h}_2, \dot{h}_3]$	= Tilted wheel torque (in W)
$\boldsymbol{h} = [h_1, h_2, h_3]$	= Tilted wheel angular momentum (in W)
J_w	= Tilted wheel inertia
$\left[\chi_B^I\right] = [\phi, \theta, \psi]$	= Air-bearing table attitude (in B)
Ω_w	= Tilted wheel speed
u	= Input signal (generic)
$[u_\alpha, u_\beta, u_\Omega]$	= Tilted wheel control signals
$[u_\phi, u_\theta, u_\psi]$	= Air-bearing table control signals
W	= Tilted wheel body frame

1. Introduction

There are several existing actuators which can be used to alter the attitude of a satellite inertially. Two common actuators are the Momentum Wheel (MW) and Reaction Wheel (RW). The former spins at a fixed speed and the latter at a variable speed, however neither tilt the axis of momentum generation. To achieve three-axis attitude stabilization about all three axes of a satellite, at least three reaction wheels are required. A typical RW performs an attitude manoeuvre by exchanging momentum with the satellite body and creating an internal torque, but this is limited by power requirement and size for achieving higher torque - the higher the torque required, the bigger the size, power and cost of the wheel.

An alternative class of actuator is Control Moment Gyroscopes (CMGs). These tilt the axis of momentum generation which allows torque amplification and allows a much higher torque to be produced than MWs and RWs. Unfortunately, CMGs also have singularities - a phenomenon whereby CMGs generate no torque at certain command points.

The large power requirements for MWs and RWs, and the singularity issues associated with CMGs necessitate research into other forms of control actuators that will give higher torque at lower power, mass and cost. In this research we propose a new form of actuator that uses a tilting wheel, is effectively singularity-free and has much lower power and mass requirements than a standard CMG for three-axis control. We also

*Corresponding Author. Tel.: +44 (0)1483 68 6307

Email addresses: l.o.inumoh@surrey.ac.uk (Lawrence O. Inumoh), j.forshaw@surrey.ac.uk (Jason L. Forshaw), ab3853@coventry.ac.uk (Nadjim M. Horri)

URL: www.ee.surrey.ac.uk/ssc (Lawrence O. Inumoh)

[1]Control Systems PhD Researcher, Surrey Space Centre

[2]Research Fellow (Spacecraft and GNC), Surrey Space Centre

[3]Lecturer in Aerospace Engineering, Coventry University

underline the dynamics for the system and propose a control law that is suitable for its usage.

1.1. Literature

The use of CMGs started in the 1960s for use in Skylab [1] and its high precision payload ATM. This study encompassed both hardware and software that is responsible for the control and steering of the CMG. Design of steering logic for the avoidance of singularities associated with CMGs during operation became an active research area. To circumvent the problems posed by singularity issues, Nakamura [2] first proposed singularity robust logic for single gimbal control moment gyroscopes (SGCMGs) while Wie [3] modified this steering logic by introducing a simple minimum two norm pseudo-inverse solution. The proposed singularities robust logic could not eliminate singularities but provided 'deterministic dither signals' when the SGCMG system approached a singularity. In solving the singularity problems associated with SGCMGs and variable speed control moment gyroscopes (VSCMGs), Schaub [4] used a weighted minimum norm inverse to determine the control vector which allows the VSCMG to operate like a conventional reaction wheel or CMG depending on the used control logic.

Lappas's [5] work also took precedence from Busseuil's [6] work that provided description of a mini CMG developed in Alcatel that used magnetic bearing technology for attitude control accuracy improvement. Pechev [7] in his work proposed a new control approach for solving the singularity avoidance problem associated with CMGs based on the observation that the gimbal rates can be derived by minimizing (in a feedback loop) the difference between the demanded torque and the control moment gyro output torque. Ford [8] in his work also proposed a gimballed momentum wheel concept that is used for attitude control of satellite with flexible appendages. Post [9] develops a fault-tolerant sliding mode attitude control algorithm for a nanosatellite using a reaction wheel and performs tests using an air-bearing table. An air-bearing table has also been used for attitude control development in [10]. The latest research concerning CMGs is the work by Stevenson and Schaub [11, 12] that developed a mathematical model for the operation of a double-gimbal variable speed CMG (DGVSCMG) from control analysis concept. Schaub's work added some terms to the inner loop controller to compensate orbit frame conversion terms (those terms can also cause singularities otherwise) to maintain singularity at 90°.

1.2. The Proposed Actuator

The proposed actuator as shown in Figure (1) focuses on the use of one spinning wheel and tilt mechanism to generate torque in all three axes of a rigid satellite. Unlike a DGVSCMG [11], the actuator is mounted on flat plate which allows the mounting of RWs or MWs to the plate. Additionally, the tilt mechanism is not constrained to use rotary motors - linear motors could also be used for tilt control. Further advantages include less mass, volume, and greater simplicity than other actuators. The tilted wheel allows full three-axis control of a satellite unlike a DGCMG that only allows two-axis control by itself. Clever formulation of equations of motion for the system allow the actuator to be effectively singularity-free, a key breakthrough from past literature. This is done by moving the singularities to tilt angle locations that would not be practical in nominal operation. The development of the tilted wheel mathematical model and simulation of the tilted wheel is developed in past research [13, 14].

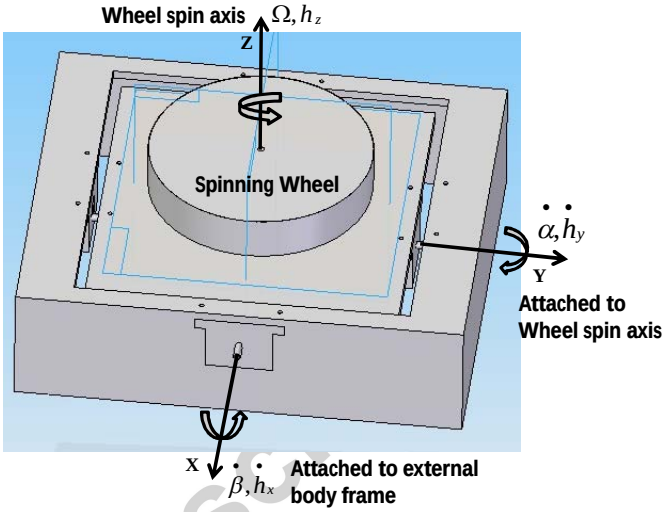

Figure 1: Proposed Tilted Wheel (combined A-1 and A-2).

2. Tilted Wheel Hardware

This section describes the various components that make up the tilted wheel: the structure, motors, wheel, tilt mechanism and encoders. The tilted wheel prototype is shown in Figure (2).

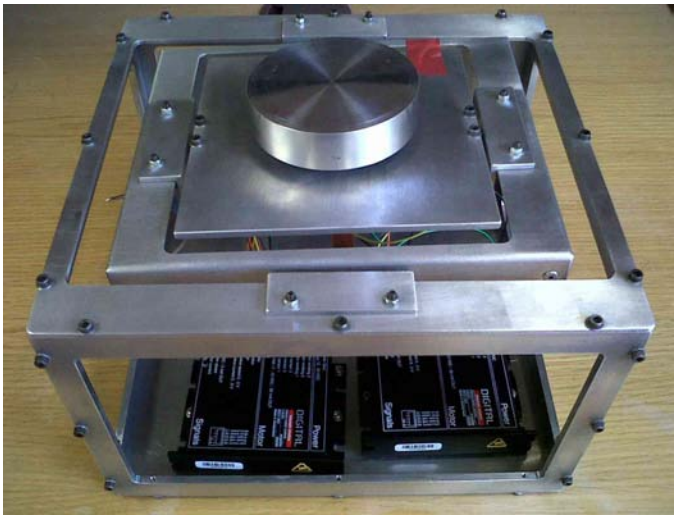

Figure 2: Image of a manufactured Tilted Wheel (combined A-1 and A-2). Measuring $250 \times 230 \times 150$ *mm*.

2.1. Structure

The built prototype is composed of a brushless DC motor, a pair of stepper motors and a pair of incremental encoders. The selection and use of stepper motors for the tilt mechanism is to keep the design simple and reduce the overall mass. More information about the individual components used are discussed in the next sections. Also used to ensure smooth performance and structural integrity of the design are ball bearings that provide pivotal and structural support to each of the tilt axes. Couplers are also used to support and secure the ball bearings to the tilted wheel main structure and also to support and secure the shaft that holds the encoders. The mechanical frame is made of square stainless steel metal plate that denote the principal mechanical axes.

2.2. Flywheel

Based on the tilted wheel angular momentum envelope described in [15], the spinning wheel (flywheel) must be able to store angular momentum up to 0.46 Nms. This amount of angular momentum stored by the spinning wheel is dependent on its rotation rate and the rotational inertia. The spinning wheel is rotated by a high speed BLDC motor (Maxon EC 45 flat ⌀42.9 mm, brushless, 30 W flat motor) with integrated hall sensor that enhances the motor commutation.

For simplicity, the flywheel (made of stainless steel material (304) with a density of 8000 kgm^{-3}) dimension is generated based on the system required angular momentum of 0.46 Nms and assuming that the minimum angular velocity of the motor is 575 RPM, the moment of inertia for the flywheel is calculated using Equation (1) where H_{fw} is the flywheel angular momentum, Ω_{fw} is the spinning wheel minimum angular velocity and J_{fw} is the flywheel moment of inertia.

$$H_{fw} = J_{fw} \cdot \Omega_{fw} \tag{1}$$

2.3. Motors

The tilted wheel is made up of three major assemblies that has two tilt mechanisms. The first two assemblies (inner and the outer tilt mechanism respectively) are responsible for tilting the spinning wheel while the third assembly is the structure that holds the stepper motor that rotates the outer tilt mechanism. The third assembly also serves as the primary structure for the the tilted wheel and an interface to the satellite body. The inner mechanism (Assembly-1 or A-1) comprises the flywheel, the inner plate that carries the spinning wheel, the brushless DC motor, and the mounting brackets. The total mass of A-1 is 0.473 kg. The outer assembly (Assembly-2 or A-2) is made up of the total mass of the A-1, A-2 frame, stepper motor 1 (that rotates A-1), incremental encoder that measures A-1 rotation, and the mounting brackets for A-1.

To determine the minimum required torque for a stepper motor, values of the following torque components must be known for each assembly part that is rotated by each stepper motor and Newton's second law is the basic equation used for this computation.

$$N = N_{fric} + N_{inertia} \tag{2}$$

2.3.1. Friction

The initial friction (stiction) torque component must be overcome and thereafter sustain the drive against the friction of A-1 and against any other cutting forces. The frictional component of the torque and force are given by Equations (3) and (4) respectively where r is the radius of the shaft connecting A-1, e is the effeciency of conversion of the rotation by the motor to rotation of A-1, F_c is the friction coefficient (kinetic) and g is the acceleration due to gravity.

$$N_{fric} = F_{fric} \cdot \frac{r}{2 \cdot \pi \cdot e} \tag{3}$$

$$F_{fric} = M_{A-1} \cdot g \cdot F_c \tag{4}$$

If the total mass of A-1 is calculated to be 0.473 kg, and the friction coefficient F_c is assumed to be 0.2 for cast iron, using Equation (4), the frictional force F_{fric} is calculated to be 0.927 N.

The efficiency of conversion of the rotation by the stepper motor to rotation of the A-1 (e) is taken as 95%. The torque friction component then becomes 0.38 mNm (milli Nm).

2.3.2. Tilt Mechanism Sizing

The Inertia torque component (the tendency of A-1 to remain at rest) must be overcome. This is true even if the friction force is zero. The moment of inertia, J_{A-1}, of A-1 obtained from the CAD model is 3.2×10^{-5} kgm^2. There must always be a correlation between the speed of the moving part and the ideal acceleration to avoid losing steps, but must give rapid direction change for accuracy. For the stepper motor sizing, the acceleration phase is assumed to happen within the first full step of the stepper motor (0.1 ms), and if the maximum required angular velocity is 7°s^{-1} (0.122 rads^{-1}). The acceleration is therefore calculated as 1220 rads^{-2}. The torque required to achieve the calculated acceleration against the inertia load is calculated using Equation (5) and is 39 mNm.

$$N_{inertia} = J_{MP-1} \cdot Acc \tag{5}$$

The total torque component is calculated to be 39.3 mNm. The calculated total torque component is multiplied with a design factor of 2. So, the minimum holding torque required for stepper motor-1 to rotate A-1 at the required maximum angular velocity will be 78.6 mNm.

Similar to how the stepper motor for rotating the A-1 was sized, same concept was used to determine the minimum holding torque required to rotate the A-2. Using Equations (2), (3), and (5), the total torque component for stepper motor-2 is calculated to be 73.17 mNm. Multiplying the total torque components with a factor of 2, the minimum holding torque required by a stepper motor that will rotate A-2 at the required maximum tilt rate of 7°s^{-1} will be 146.34 mNm. Based on the availability, a 60 mNm Nema 11 DC Stepper Motor (11HS12-0674S) and a 230 mNm Nema 14 DC Stepper Motor (14HS17-0504S) were selected for A-1 and A-2 respectively.

2.4. Encoder

In order to accurately compensate for any motion error in the tilt mechanism, the exact tilt angle must be known. Since the Nema stepper motor used does not provide position feedback, the attached incremental encoder will have to directly measure the tilt shaft and feedback the measurement into the system to minimise or remove the motion error due to the stepping of the stepper motors. An HEDS-9100 A14 two channel optical encoder that works with code wheel HEDS-5120 A14 that has a resolution of 500 CPR (counts per revolution).

3. Standalone Testbed

3.1. Testbed Setup

The standalone testbed describes the bench level test carried out on the tilted wheel to determine the functionality of both the tilt mechanism and the spinning wheel. This test involves open loop control of the stepper motors and the brushless DC (BLDC) motor that rotates the spinning wheel to show their tilt capabilities in achieving various tilt angle setpoints. Figure 3 shows how the components are connected in the simplified testbed.

The I/O cards used are National Instruments PCI 6024E and PCI 6703 which are high speed data acquisition cards with an array of analogue and digital I/O. For the standalone testbed, commands and telemetry for the operation of all the tilted wheel components especially the spinning wheel are initiated from the host PC, received by the PCI 6024E via the connected R6868 Ribbon cable.

The PCI 6703 card is used to send several control commands: (a) to drive the BLDC motor, (b) to set the spinning wheel direction, (c) setting the Enable command that is responsible for initiating the turn on of the control driver. Telemetry that shows the functionality of the BLDC motor is also received through PCI 6024E card. Two major pieces of information required are: (a) the wheel speed and (b) the current drawn by the BLDC motor. The PCI 6703 card was selected for driving the BLDC motor due to availability of about 16 analogue output channels while PCI 6024E has a limited number of analogue output channels to support our requirement.

The PCI 6024E card has 8 digital I/O channels that can be configured to either operate as input channels or output channels depending on the requirement. Both the commands to drive stepper motor-1 and to set the stepper motor-1 direction are sent from the host PC through the PCI 6024E digital channels. Another set of digital output channels are allocated for the control of the second stepper motor.

Part of the unused digital channels were also configured to read the tilt angles and rates measurement by the encoders. A set of both encoder and code wheel is mounted directly to each of the wheel's x-axes and y-axes to provide the direct tilt angle about the tilted wheel x-y plane. The PCI 6024E digital channels 19, 51, 16, and 48 were configured to measure the digital readings of Encoder-1 channels A and B and Encoder-2 channels A and B respectively.

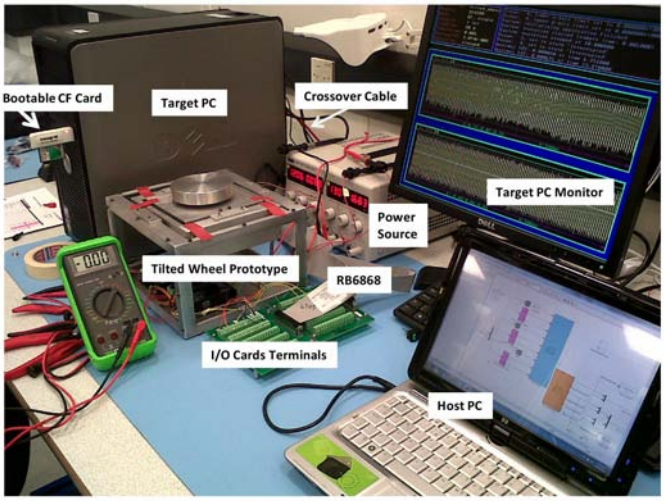

Figure 3: Standalone Testbed Setup

The standalone test plan is to verify the tilt capability of the stepper motors in achieving three different tilt angles setpoints of α and β. Also verified in this test plan is the performance of the tilt mechanisms at both fixed and variable spinning wheel speeds.

3.2. Results and Discussion

The open loop control of the tilt mechanism at spinning wheel fixed speed showed repeatability in achieving the tilt angle setpoints with both roll and pitch signals including the control signals showing some consistency as shown in Figures 4 and 5 respectively. Figure 4 shows the results for pitch at three different setpoints: [5° 10° 15°]. Each of the three setpoints is repeated three times to guarantee no coincidences. The error in pitch is on the order of 1° or less. Figure 5 shows the results for roll over the same setpoint range. The error ranges from 0.5° to 2°.

The same tilt angle setpoints were commanded with variable spinning wheel speed of 100 RPM, 500 RPM, 1000 RPM, and 1500 RPM respectively for both roll and pitch command. Figure 6 [A] showed some offset from the roll setpoints due to the stepper motor insuffcient holding torque that resulted in jittering at lower spinning wheel speed. But the pitch axis setpoints showed consistency even at a lower spinning wheel speed because of the stepper motor aligned to the axis has sufficient holding torque that is able to support the spinning wheel at different speed during commanded tilt angles. By and large, the step angle error of about 1° in the stepper motor contributed to the setpoint error observed.

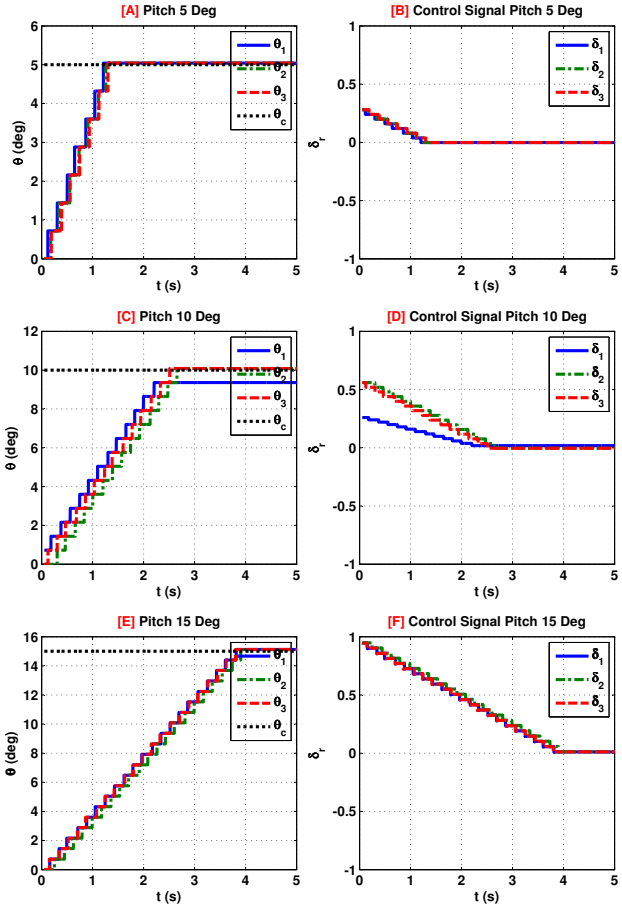

Figure 4: Standalone Testbed Results: Pitch (5° 10° 15°).

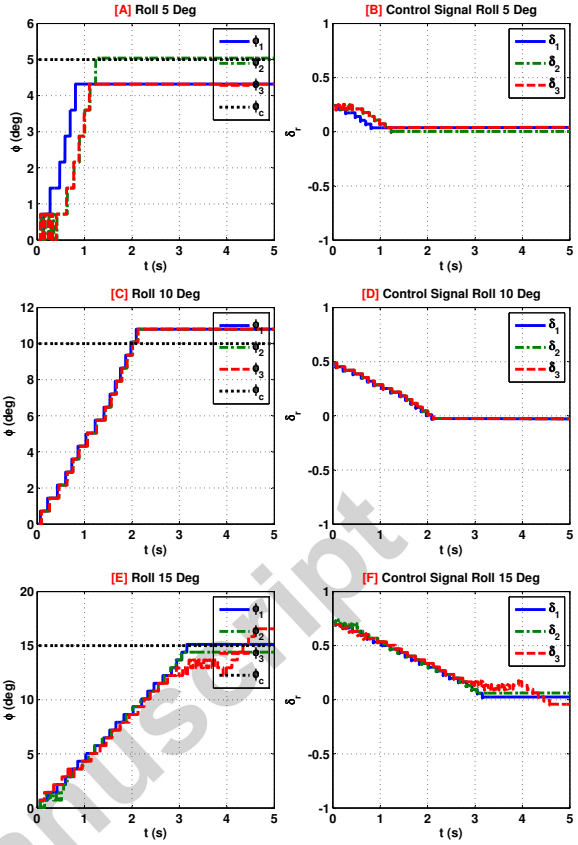

Figure 5: Standalone Testbed Results: Roll (5°, 10°, 15°).

4. Air-Bearing Table Testbed

4.1. Testbed Setup

The air-bearing table (ABT) is made up of an air bearing head shown in Figure (7) that is a disk-shaped platform suspended by compressed clean air from an external source through series of control valves that regulate the air flow in the system. The ABT allows the rotation of the platform and all components mounted or attached without significant friction about ±30° about the roll and pitch axes and 360° about the yaw axis. It is used to test the dynamic characteristics and performance of a model satellite control system throughout an ACS module bench test campaign. The ABT allows simulation of near zero-g of space environment when its centre of gravity coincides with the centre of rotation of the rotating platform.

The hardware architecture can be seen in Figure 8. Some of the components available on the table are: an attitude sensor (inertial measurement unit - IMU) that helps to determine the angular movement of the table from its inertial position in all three axes of a representative satellite, a wireless communication link and an integrated harness system that includes the power connector and the signal interface, PCM 3375 (is a low cost PC104 that has Enhanced IDE interface supports, One serial RS-232 port) that is used as the OBC to interface all compo-

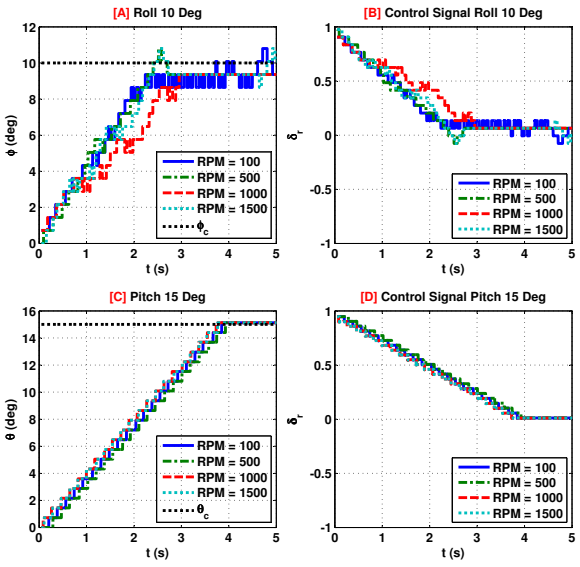

Figure 6: Standalone Testbed Results: Operational Wheel.
This figure shows the results for the roll axis at 10° and the pitch axis at 15° with the wheel moving. The experiments have been conducted at 4 different RPMs: 100, 500, 1000, 1500.

nents on the ABT and the tilted wheel, an I/O card (DMM 32X AT) that sends and receives analogue and digital input and output signals from the OBC and the tilted wheel components. The tilted wheel prototype is also firmly mounted on the air-bearing table while commands are sent to it from the Matlab/Simulink model on the host computer through the TCP/IP wired communication link available. Also, available on the ABT as shown in Figure (7) is a mass balancing mechanism made of several types of mass that help to maintain the platform balance by ensuring equilibrium between the total mass above the spherical ball (on top the ABT platform) and the balancing masses below the suspended ball.

Compressed and clean air pressurised to a maximum value of 50.76 psig or 3.5 bar is supplied to the ABT from an external source through a control valve. At a preset maximum pressure, the ABT floats easily and settles down within a reasonable time frame when tilted or perturbed about the roll and pitch plane.

To demonstrate the three degrees of freedom capability of the tilted wheel, the air-bearing table facility will be used in the second test campaign where the controlled platform attitude will be fed back into the control system for proper determination of the performance of the tilted wheel.

4.2. Control Architecture Setup

The newly developed dynamic equation of motion for the proposed inertial actuator as contained in [14] described the formulation of the mathematical models. But in practice the generated torque is decoupled for easy and simplified implementation, while the spinning wheel speed is set at 2700 RPM. The decoupled equation is represented in Equation 6.

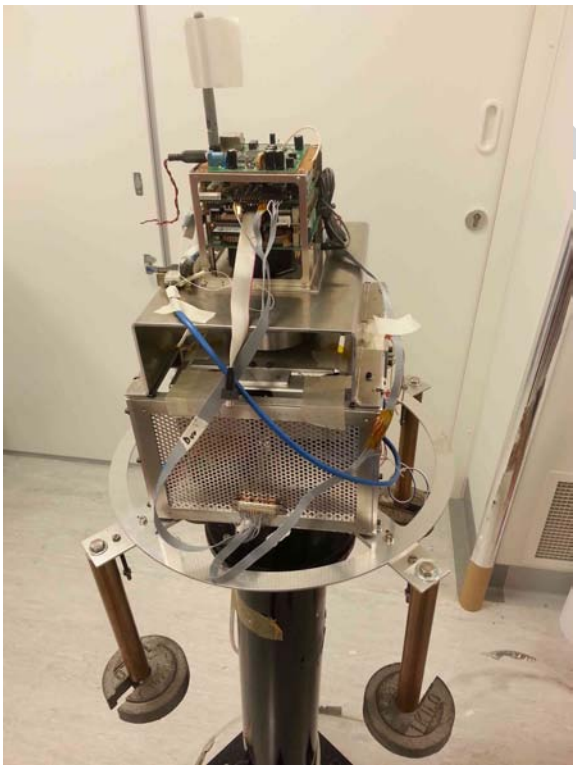

Figure 7: Air-Bearing Table Testbed: Setup. Figure shows the overall air-bearing table setup. The tilted wheel is mounted on top of the air-bearing podium. The CubeSat is mounted on top of the tilted wheel with an adapter plate. The mass balancing mechanism can be seen as a series of additional weights suspended from the table.

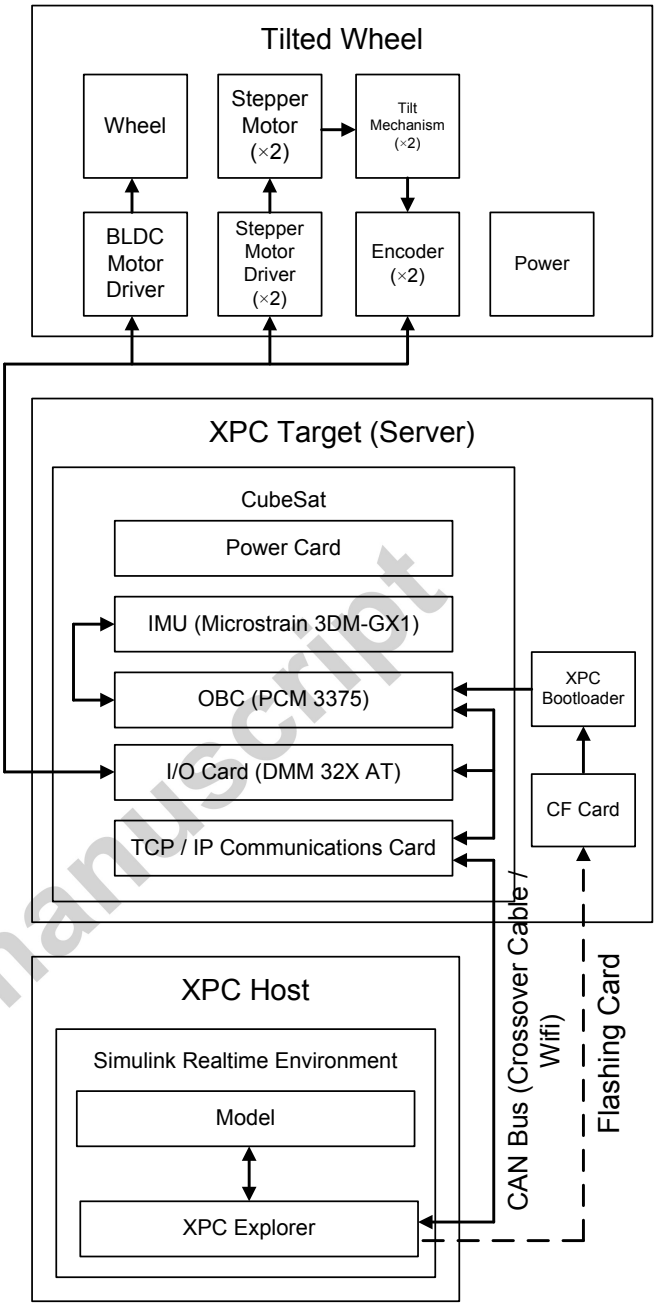

Figure 8: Air-Bearing Table Testbed: Hardware Architecture. Figure shows how the power and the signal channels are connected between the CubeSat, tilted wheel and Host PC

$$\dot{\boldsymbol{H}} = \begin{bmatrix} \dot{\alpha} J_w \Omega_w \cdot \sin\alpha \sin\beta - \dot{\beta} J_w \Omega_w \cdot \cos\alpha \cos\beta - \dot{\Omega} J_w \cdot \cos\alpha \sin\beta \\ \dot{\alpha} J_w \Omega_w \cdot \cos\alpha + \dot{\Omega} J_w \cdot \sin\alpha \\ -\dot{\alpha} J_w \Omega_w \cdot \sin\alpha \cos\beta - \dot{\beta} J_w \Omega_w \cdot \cos\alpha \sin\beta + \dot{\Omega} J_w \cdot \cos\alpha \cos\beta \end{bmatrix} \quad (6)$$

The ABT experimental setup is to demonstrate the 3-DoF capability of the built actuator, especially in torque generation

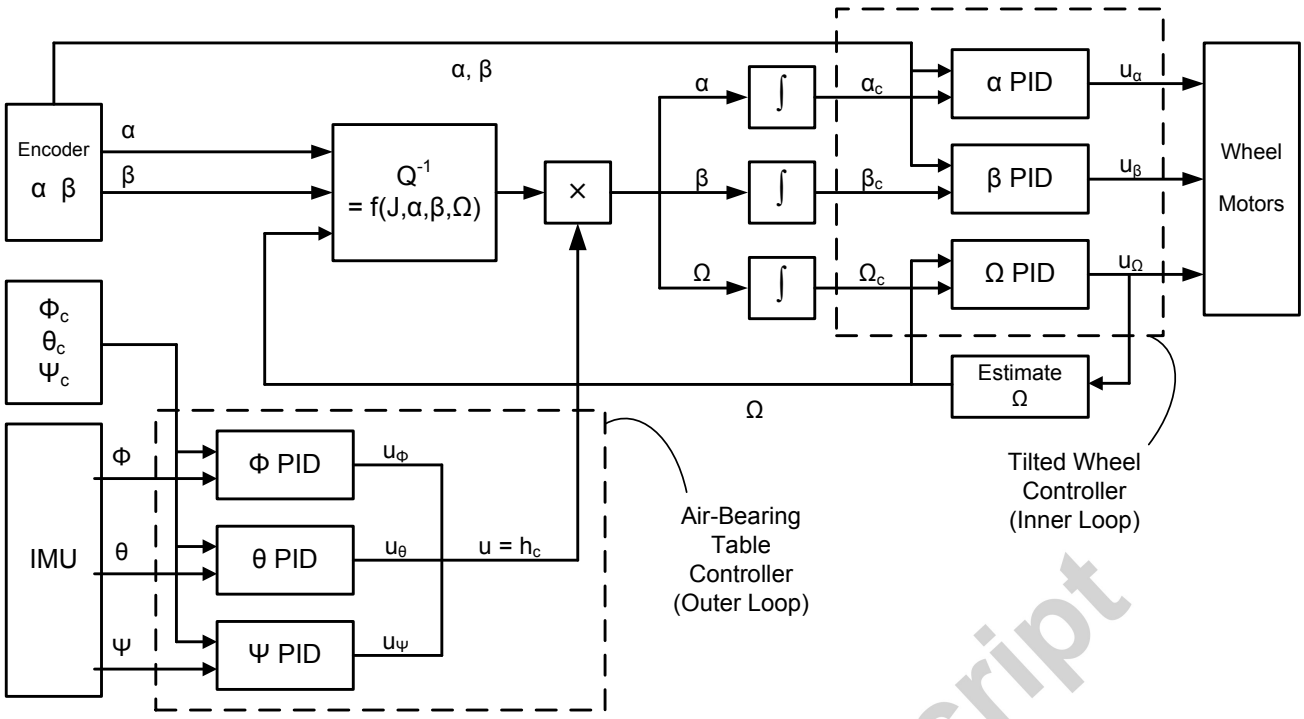

Figure 9: Air-Bearing Table Testbed: Control Architecture. Figure shows the control architecture for the air-bearing table testbed. Subscript *c* indicates a setpoint command, *u* indicates a control signal. The setpoint commands for the air-bearing table are given by the user; the setpoint commands for the tilted wheel (inner loop) are computed from the output of the $\boldsymbol{Q}$ inversion process and the output of the air-bearing table outer control loop.

about the roll and pitch plane axes, where the tilted wheel concept of torque amplification similar to that obtainable in the CMGs systems is demonstrated.

Based on the testbed control architecture shown in Figure 9, the tilt mechanism control command is determined by the interaction between the commanded torque from the ABT controller and the inverted $\boldsymbol{Q}$ matrix computed using the spinning wheel speed, the moment of inertia (MoI), and the tilt angles measured by the encoders as presented in Equation 7.

$$\begin{bmatrix} \dot{\alpha} \\ \dot{\beta} \\ \dot{\Omega}_w \end{bmatrix} = \begin{bmatrix} J_w\Omega_w & 0 & 0 \\ 0 & J_w\Omega_w & 0 \\ 0 & 0 & J_w \end{bmatrix}^{-1} \boldsymbol{Q}^{-1}\dot{\boldsymbol{h}}_c \tag{7}$$

The tilt mechanism and the spinning wheel speed control command of Equation (7) can be written in the components form as:

$$\begin{bmatrix} \dot{\alpha} \\ \dot{\beta} \\ \dot{\Omega}_w \end{bmatrix} = \begin{bmatrix} \frac{1}{J_w\Omega_w}\left(\sin\alpha\sin\beta\cdot h_{c1} + \cos\alpha\cdot h_{c2} - \sin\alpha\cos\beta\cdot h_{c3}\right) \\ \frac{1}{J_w\Omega_w}\left(-\frac{\cos\beta}{\cos\alpha}h_{c1} - \frac{\sin\beta}{\cos\alpha}h_{c3}\right) \\ \frac{1}{J_w}\left(-\cos\alpha\sin\beta\cdot h_{c1} + \sin\alpha\cdot h_{c2} + \cos\alpha\cos\beta\cdot h_{c3}\right) \end{bmatrix} \tag{8}$$

The tilted wheel MoI used was generated by the CAD SolidEdge modelling of the actuator and is given as 0.0008 kgm^2. In reality, the actual MoI might be greater than this considering other components added to the system such as the motor drivers and the harness system.

There are two sets of PID controller used in the control architecture as shown in Figure 9. The first controller is the outer PID controller used for the control of the ABT platform that uses the attitude error between the attitude setpoint and the IMU measurement to compute the torque command for the control of the air-bearing platform. The PID gains were tuned using the Ziegler Nichols tuning method [16]. The inner PID controller (tilt mechanism controller) generates the torque command for the operation of the tilt mechanism by computing the tilt error between the measured tilt angles by the encoders and the commanded tilt angles got from the interaction of the commanded torque and the inverted $\boldsymbol{Q}$ matrix. The inner and outer loop gains can be seen in Table 1.

Table 1: Air-bearing Table Gains. Table shows the gains in the inner and outer loop PID controllers for the air-bearing table. † Inner loop yaw is estimated from the yaw controller output. * RPM per volt.

Variable	P	I	D
Outer Loop			
ϕ	1.2	1.3	2.5
θ	1.2	1.3	2.5
ψ	3	0.1	0.0035
Inner Loop			
α	0.0039	0.0312	0.0122
β	0.0039	0.0312	0.0122
$\Omega^\dagger$	750*		

4.3. Results: Roll and Pitch (Sample Case)

Figures 10 to 12 show the results for the ABT testing. Figure 10 shows the results for the air-bearing table (outer loop). Two different experiments are commanded: in the first, $\phi = 2°$, $\theta = 3°$ is commanded; in the second $\phi = 4°$, $\theta = 1°$ is commanded. On Earth, the air-bearing vertical centre of gravity is not 'perfectly balanced' resulting is a slight restoring moment on the roll and pitch axes (naturally, this is not an issue in space with no gravity). This means only small roll and pitch setpoints are used to prevent saturation occurring.

The tilted wheel was able to manoeuvre the table close to the setpoints as measured by the IMU. Figure 10[A] shows that the setpoints of $\phi = 2°$, $\theta = 3°$ were attained within a 0.5° error. The error source was an initial reading by the IMU due to table imbalance and other error sources. It is to be noted that large manoeuvres are better tracked than smaller ones because the effect of error sources is more significant in the case of small manoeuvres. In Figure 12[C], the initial IMU measurement of 0.7° about the table pitch axis (the $\theta = 1°$ setpoint) was largely responsible for the attitude error. The results for how the tilt mechanism moves during these experiments can be seen in Figures 11[A] and [B].

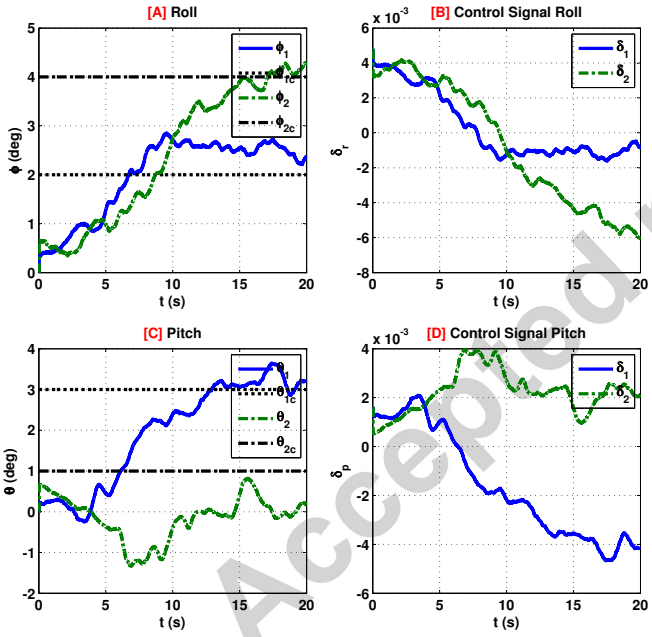

Figure 10: Air Bearing Table Testbed Results: Roll and Pitch.
This figure shows the results for the roll and pitch axes (on the table). The first experiment commands: $\phi = 2°$, $\theta = 3°$; the second commands: $\phi = 4°$, $\theta = 1°$. Both control signals are shown.

Figure 12 shows the wheel speed during the experiment. The experimental setup did not use a dedicated power supply (such as batteries) but was powered from a digital power supply that is connected to the setup with cables that were passed through the ceiling. This arrangement was a source of error to the setup as evident in the results shown below. A little disturbance to the overhead cables results in a large disturbance torque especially

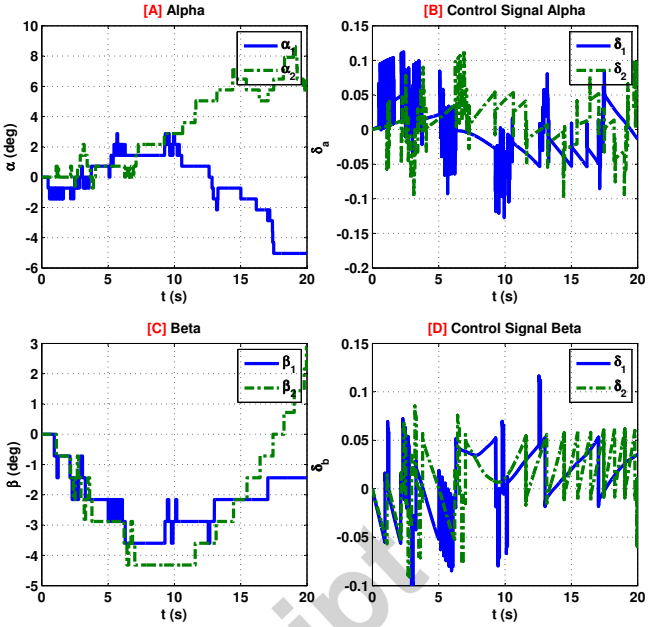

Figure 11: Air Bearing Table Testbed Results: Alpha and Beta.
This figure shows the results for the tilting axes (on the tilted wheel). Both control signals are shown. The experiments correspond with those seen in Figure 10.

about the roll and pitch angles. Though the ABT is controlled through a feedback control mode, that exerts more control command on the spinning wheel and the tilt mechanism, the consequence of this error will easily saturate the spinning wheel nominally. This was responsible for operating the spinning wheel at a set speed of 2700 RPM to avoid problems associated with the spinning wheel saturation in the tilted wheel dynamic equation.

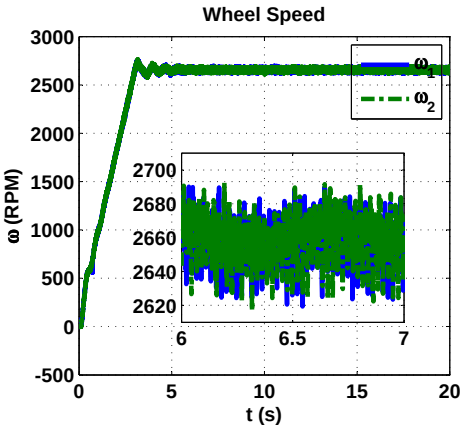

Figure 12: Air Bearing Table Testbed Results: Roll and Pitch Experiment Wheel Speed.
This figure shows the results for the wheel speed in RPM during the roll and pitch experiment. The experiments correspond with those seen in Figure 10.

The IMU measurement has inherent error about all the three principal axes, but the yaw attitude measurement was not as good as both roll and pitch measurements. This is because, the yaw measurement is obtained from a compass within the IMU,

which was highly sensitive to external magnetic fields in the laboratory, including the ones from the motors used. But the yaw attitude can easily be achieved by changing the spinning wheel speed accordingly.

4.4. Results: Yaw (Sample Case)

The yaw attitude test completed examination of the 3-DoF capability of the tilted wheel. As can be seen from Figures 13 and 14, the yaw manoeuvre is achieved by varying the speed of the spinning wheel. The setpoint is set to $\psi = 13°$ in this scenario. The setpoint attitude was achieved in less than 17 s settling time while the control signal responsible for the yaw axis control has a minimum value of -0.6.

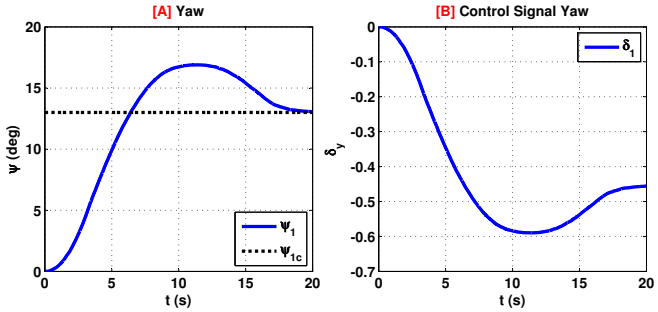

Figure 13: Air Bearing Table Testbed Results: Yaw.
This figure shows the results for the yaw axis (on the table). The experiment commands: $\psi = 13°$. The control signal is shown.

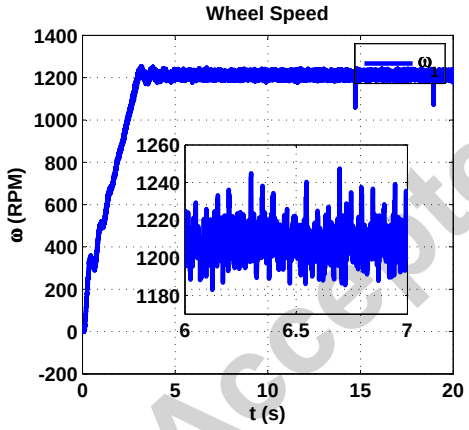

Figure 14: Air Bearing Table Testbed Results: Yaw Experiment Wheel Speed.
This figure shows the results for the wheel speed in RPM during the yaw experiment.

4.5. Results: Roll and Pitch (Repeatability)

To show the repeatability of the test results, some commanded setpoints for roll and pitch manoeuvres were repeated several times with three of the results plotted. The plotted profiles in Figures 15 and 16 show a roll manoeuvre for the setpoint of $\phi = 2°$ and a pitch manoeuvre for a setpoint of $\theta = 3°$. The results show that regardless of the initial condition of the platform (in either roll or pitch), the tilted wheel causes the air bearing table to converge to the desired setpoint with a small

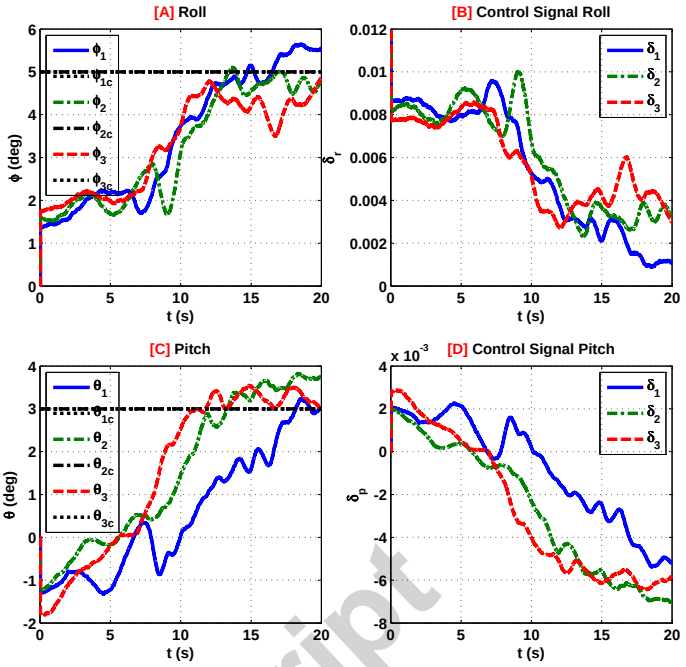

Figure 15: Air Bearing Table Testbed Repeatability Results: Roll and Pitch.
This figure shows three repeated results for the roll and pitch axes (on the table) for $\phi = 5°$, $\theta = 3°$.

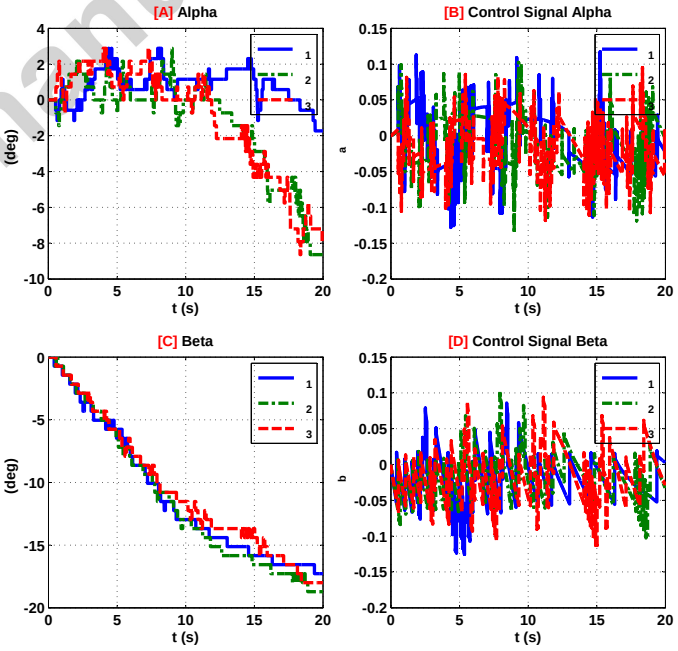

Figure 16: Air Bearing Table Testbed Repeatability Results: Alpha and Beta.
This figure shows three repeated results for the tilting axes (on the tilted wheel). The experiments correspond with those seen in Figure 15.

setpoint error. Additionally the maximum tilt angle recorded for the repeated pitch manoeuvres is 8.5° showing that the tilted wheel can generate the required torque with admissible tilt angles.

4.6. Results: Roll and Pitch (Regulation)

Figure 17 shows the tilted wheel's ability to regulate the table to the origin. This shows an inherent ability for the tilted wheel to stabilise the air bearing table (satellite).

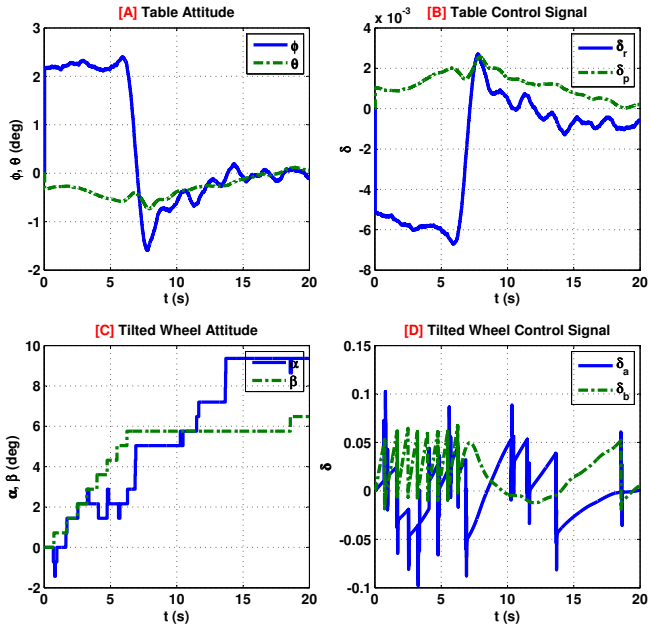

Figure 17: Air Bearing Table Testbed Regulation Results.
This figure shows the ability of the tilted wheel to regulate the air bearing table to a 0° setpoint.

With the table having an initial attitude of 2.5° and 0.15° about the roll and pitch axes respectively, the table was commanded to settle to the origin, i.e. setting both roll and pitch to 0°. This was achieved in less than 15 s with tilt angles of approximately $[9, 7]°$.

4.7. Sources of Error

The air-bearing testbed is influenced by several different error sources which are very hard to quantify. From an air-bearing table perspective, scratches on the platform lead to a lack of a completely frictionless surface. A gravity gradient torque can also be seen in the results caused by the necessary wires attached from the ceiling to the air-bearing platform. In addition an aerodynamic disturbance is present due to the room air conditioning system that ensures a clean air supply and an ambient environment free from dust and dirt. From a mechanical perspective, the wheel spindle is offset from the centre of mass of the system slightly due to manufacturing tolerances. Additionally, the motor is only accurate to 1.5° meaning aligning the table at exactly 0° at the start of an experiment is difficult.

5. Comparison to Alternative CMG Systems

This section aims to quantify the aforementioned claims that the Tilted Wheel provides full 3-DOF control yet requires less power and mass than a conventional CMG system.

5.1. Attitude Degrees of Freedom

The number of degrees of freedom for various CMG systems can be seen in Table 2. It can clearly be seen that with just two Tilted Wheels full redundancy is provided over all attitude degrees of freedom. The pyramid configuration also offers this redundancy at added complexity, mass and power, having 4 SGCMG wheels. The other configurations can offer no such redundancy without the addition of further momentum wheels.

Table 2: Attitude Degrees of Freedom. Table shows the numbers of degrees of freedom for various CMG systems including redundancy options. † For configuration, axis can be either roll or pitch (but not both).

Configuration	Main			Redundant		
	ϕ	θ	ψ	ϕ	θ	ψ
1 × Tilted Wheel	√	√	√	-	-	-
2 × Tilted Wheel	√	√	√	√	√	√
1 × SGCMG†	√	-	-	-	-	-
2 × SGCMG†	√	-	-	√	-	-
1 × DGCMG	√	√	-	-	-	-
2 × DGCMG	√	√	-	√	√	-
1 × VSCMG†	√	-	√	-	-	-
2 × VSCMG†	√	-	√	√	-	√
1 × DGVSCMG	√	√	√	-	-	-
2 × DGVSCMG	√	√	√	√	√	√
Pyramid (4 × SGCMG)	√	√	√	√	√	√

5.2. Power and Mass

The average power usage for the Tilted Wheel can be calculated as the combined power usage from each piece of hardware. The BLDC motor requires 0.304 W (as can be seen from Figure 18), the two stepper motors 1.280 W and the two encoders 0.100 W, yielding an average power of 1.68 W.

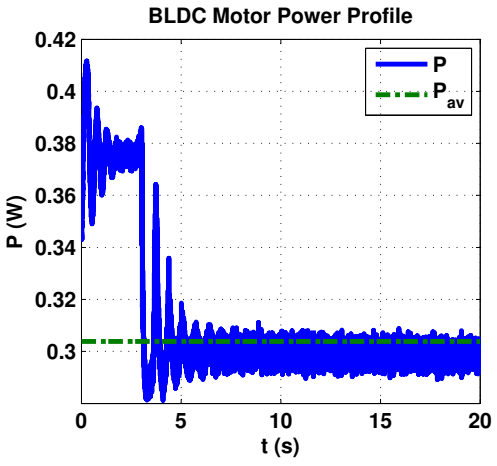

Figure 18: BLDC Motor Power Profile.
This figure shows the power requirement for the motor. The initial peak shows the starting power required to start the motor.

Comparison of specifications for some inertial actuators can be seen in Table 3. Comparison factors scaled power and scaled energy have been added to show the respective relative usage of the CMGs scaled to minimise mass and maximise torque. It is

Table 3: Power and Mass Comparison. Table shows three existing CMGs and their power and mass specifications where bold items indicate best performance. * At maximum torque. † Scaled quantities are the property times mass divided by maximum torque.

Specification	3 × UoSAT-12	3 × Tsinghua-1	3 × CMG μSat	1 × Tilted Wheel
Configuration	3-axis	3-axis	3-axis	3-axis
Mass (kg)	9.6	3.0	1.8	**1.0**
Inertia (per unit) (kg.m^2)	40	2.5	4.1	5.64
Average Power* (W)	6.00	1.35	4.83	1.68
Maximum Torque (mN.m)	20	10	52.3	**63.3**
Scaled Power† (W.kg/mN.m)	2.88	0.41	0.17	**0.03**
Manoeuvre Time (s)	200	150	20	20
Scaled Energy (J.kg/m.N.m)	576	61.5	3.32	**0.53**

clear from the comparison that the Tilted Wheel has the least mass, requires less scaled power and energy and produces both higher torque (and angular momentum) than previous CMG actuation strategies.

5.3. Scalability

The tilted wheel system can be scaled for use with satellites in all orbits especially the Low Earth Orbit (LEO) with a size of Cubesat to small satellites. Though the built model is sized and intended mainly for LEO satellite of about 90 kg mass, it can potentially be used for attitude control of satellites or space platforms in higher orbits. The fight model of the actuator must be subjected to space environment testing before use onboard any satellite. The components used for the build of the tilted wheel are also available in smaller or larger sizes for a possible scalability of the actuator for use on a smaller or larger platform respectively. While the system structure is mainly determined by the sizes of the components driven by the subsystem requirements, the two inner moving parts must be able to achieve a 90° tilt angle without restriction or limitation by the outer Assembly or the harness.

5.4. Comparison to DGVSCMG

Although both the DGVSCMG and Tilted Wheel provide 3-DoF control, the Tilted Wheel has several advantages. Firstly, the Tilted Wheel allows for a conventional reaction wheel or any other type of angular momentum generator to be mounted on the flat plate carrying the spinning wheel, as opposed to a DGVSCMG which only accommodates a spinning wheel. The gimbals used in DGVSCMG (or other type of CMG systems) are relatively complex in design and heavier than the Tilted Wheel mechanism. Finally a failure of any of the gimbal systems will render a whole DGVSCMG system inoperable, in contrast to the Tilted Wheel which will still guarantee 2-DoF in the case of a failure of one of the tilt mechanisms.

6. Conclusions

A novel inertial actuator has been proposed as a new approach to achieve three-axis attitude control of a satellite. Previous research in [14] explored the mathematical development and simulation of the Tilted Wheel; this paper has extended that research to experimentally validate the system. Experimentation was undertaken for both a standalone testbed and a full air-bearing table testbed. The concept allows for three axis torque generation by varying the speed about the wheel spin axis and by creating a gyroscopic and amplified torque about the two other axes of the actuator relative to the roll-pitch plane of the ABT as shown in the results. It has been confirmed that the Tilted Wheel has lower power and mass requirements than existing actuation strategies.

This actuator design is a step towards the development of a new generation of momentum exchange devices with a potential for high torque generation in all three axes of a rigid satellite, with significant power, mass and cost savings than all other existing CMG strategies. This single actuator is also particularly suitable for space constrained satellites and can be seen as an alternative to conventional three wheel assemblies. The experimental setup and results has justified the performance and capabilities of the actuator as described in [14]. In conclusion, this research has greatly contributed to the state of the art in the field of actuator design for satellite attitude control systems (ACS).

[1] The, Bendix, Corp., Control moment gyroscope gimbal actuator study, Tech. Rep. AFFDRL-TR-66-158, 210p, The Bendix Corporation (November 1966).

[2] Y. Nakamura, H. Hanafusa, Inverse kinematic solutions with singularity robustness for redundant manipulator control, ASME Journal of Dynamic Systems Measurement and Control 108 (3) (1986) 163–171.

[3] B. Wie, D. Bailey, C. Heiberg, Rapid multitarget acquisition and pointing control of agile spacecraft, AIAA Journal of Guidance, Control, And Dynamics 25 (1) (2002) 96–104.

[4] H. Schaub, S. R. Vadali, J. L. Junkins, Feedback control law for variable speed control moment gyros, Journal of the Astronautical Sciences 46 (3) (1998) 307–328.

[5] V. J. Lappas, A control moment gyro (CMG) based attitude control system (ACS) for agile small satellites, Ph.D. thesis, Surrey Space Centre, University of Surrey (October 2002).

[6] J. Busseuil, M. Llibre, X. Roser, High precision mini-CMGs and their spacecraft applications, in: Proceedings of AAS Guidance and Control Advances in the Astronautical Sciences, 1998, pp. 91–107.

[7] A. N. Pechev, Feedback-based steering law for control moment gyros, AIAA Journal of Guidance, Control, And Dynamics 30 (3) (2007) 848–855.

[8] K. A. Ford, C. D. Hall, Singular direction avoidance steering for control-moment gyros, AIAA Journal of Guidance, Control, And Dynamics 23 (4) (2000) 648–656.

[9] M. A. Post, J. Li, R. Lee, Nanosatellite air bearing tests of fault-tolerant sliding-mode attitude control with unscented kalman filter, in: American Institute of Aeronautics and Astronautics Guidance, Navigation, and Control Conference, Minneapolis, US, 2012.

[10] N. M. Horri, P. L. Palmer, M. Roberts, Energy optimal spacecraft attitude control subject to convergence rate constraints, Control Engineering Practice 19 (11).

[11] D. Stevenson, H. Schaub, Nonlinear control analysis of a double gimbal variable speed control moment gyro, in: AAS/AIAA Astrodynamics Specialist Conference, Girdwood, Alaska, 2011, paper AAS 11-567.

[12] D. Stevenson, H. Schaub, Nonlinear control analysis of a double-gimbal variable-speed control moment gyroscope, AIAA Journal of Guidance, Control, And Dynamics 35 (3).

[13] L. O. Inumoh, A. Pechev, N. Horri, J. L. Forshaw, Three-axis attitude control of a satellite in zero momentum mode using a tilted wheel methodology, in: American Institute of Aeronautics and Astronautics Guidance, Navigation, and Control Conference, Minneapolis, US, 2012, pp. 2815 – 2831.

[14] L. O. Inumoh, N. M. Horri, J. L. Forshaw, A. Pechev, Bounded gain-scheduled LQR satellite control using a tilted wheel, IEEE Transactions on Aerospace and Electronic Systems 50 (3).

[15] L. O. Inumoh, A. Pechev, N. Horri, Tilted wheel for three-axis control of a rigid satellite, in: Proceedings of 1st IAA Conference on Dynamics and Control of Space Systems, Porto, Portugal, 2012.

[16] G. Franklin, J. Powell, A. Emami-Naeini, Feedback Control of Dynamic Systems, Pearson Prentice Hall, 2006.